AGU ADVANCING EARTH AND SPACE SCIENCES

JGR Oceans

Key Points:

- A novel diagnostic (latitude-oxygen streamfunction) is proposed for an integrated description of the surface-to-interior oxygen pathways
- Global meridional oxygen transport occurs in two cells driven by the AMOC (Northern Cell) and the Indo-Pacific circulation (Southern Cell)
- The Southern Ocean supplies oxygen globally through northward export of SAMW and AABW at intermediate and abyssal depths respectively

Supporting Information:

Supporting Information may be found in the online version of this article.

Correspondence to:

E. Portela,
eportelanh@gmail.com

The Ocean's Meridional Oxygen Transport

Esther Portela[1,2] ⓘ, Nicolas Kolodziejczyk[1] ⓘ, Thomas Gorgues[1] ⓘ, Jan Zika[3,4] ⓘ, Coralie Perruche[5] ⓘ, and Alexandre Mignot[5]

[1]Laboratoire d'Oceanographie Physique et Spatiale (LOPS), University Brest, CNRS, IRD, Ifremer, Plouzane, France, [2]School of Environmental Sciences, University of East Anglia, Norwich, UK, [3]School of Mathematics and Statistics and UNSW Data Science Hub (uDASH), University of New South Wales, Sydney, NSW, Australia, [4]Australian Centre for Excellence in Antarctic Science (ACEAS), University of New South Wales, Sydney, NSW, Australia, [5]Mercator Océan, Toulouse, France

Abstract Quantification of oxygen uptake at the ocean surface and its surface-to-interior pathways is crucial for understanding oxygen concentration change in a warming ocean. We investigate the mean meridional global oxygen transport between 1950 and 2009 using coupled physical-biogeochemical model output. We introduce a streamfunction in latitude-oxygen coordinates to reduce complexity in the description of the mean meridional oxygen pathways. The meridional oxygen transport occurs in two main cells: (a) the Northern Cell, dominated by the Atlantic Meridional Overturning Circulation, is nearly adiabatic in the Northern Hemisphere, and transports well oxygenated waters equatorward; (b) The Southern Cell, strongly diabatic, is shaped by the circulation in the Indo-Pacific basin, and combines the subtropical and abyssal meridional circulation cells when represented in depth-latitude coordinates. Analysis of isopycnal meridional oxygen transport shows that the northward flow from the Southern Ocean transports well oxygenated waters within intermediate and bottom layers, while oxygen-rich waters reach the Southern Ocean within deep layers ($27.6 < \sigma_0 < 27.9$ kg m^{-3}), carried by the North Atlantic Deep Water (NADW). This oxygenated NADW loses around 25% of its oxygen concentration along its meridional journey from the North Atlantic (at 55°N) to the Southern Ocean. These insights into the oxygen dynamics as driven by the meridional overturning circulation provide a new framework for future studies on ocean deoxygenation.

Plain Language Summary Understanding how oxygen is transported in the ocean is important for knowing how global warming affects its concentration. In this study, we examined the mean global oxygen transport from 1950 to 2009 using a physical-biogeochemical model. We used a new latitude-oxygen coordinate system to assess how different components of ocean circulation transport oxygen throughout the global ocean. We found that there are two main oxygen pathways in the ocean, the so-called Northern and Southern cells. The Northern cell mainly influenced by the Atlantic Ocean, moves well-oxygenated water from the Northern Hemisphere toward the equator. The Southern cell, influenced by the Indo-Pacific basin, is more complex, and transports oxygen in both subtropical and deep ocean currents. By analyzing the oxygen transport along density levels, we discovered that the Southern Ocean supplies oxygen to the global ocean in intermediate and abyssal ocean layers, while it receives oxygenated waters from the North Atlantic in deeper layers above the abyss. The latter loses about 25% of its oxygen during its journey from the North Atlantic to the Southern Ocean. These findings shed light on how oxygen is distributed in the ocean and can help guide future research on ocean deoxygenation.

1. Introduction

The distribution of dissolved oxygen (DO) in the ocean results from the interplay between seawater temperature, ocean circulation, and biological processes (i.e., photosynthesis and respiration) (Brandt et al., 2015; Keeling et al., 2010). The most important control on oxygen concentration of mixed layer waters is the oxygen solubility, which decreases as seawater temperature increases. Oxygen concentration below the surface is largely determined by the mixed layer conditions at high latitudes during winter, when deep and bottom waters are formed (Feucher et al., 2022; Jacobs, 2004), and at mid-latitudes during Mode Water formation and subduction (Hanawa & Talley, 2001; Herraiz-Borreguero & Rintoul, 2011; McCartney & Talley, 1982; Portela, Kolodziejczyk, Maes, et al., 2020; Portela, Kolodziejczyk, Vic, et al., 2020). Away from the formation sites, in a hypothetical steady ocean, the oxygen distribution at any given point below the euphotic zone is determined by a balance between oxygen supply and consumption through biological respiration (Karstensen et al., 2008). This difference between

the oxygen concentration at its saturation value $\left(O_2^{sat}\right)$ and the locally measured oxygen concentration is known as the Apparent Oxygen Utilization ($AOU = O_2^{sat}\text{-}O_2$), which is expected to increase with water-mass age. Oxygen consumption is mostly driven by bacterial oxidation of organic matter near the surface. A higher consumption rate is found beneath regions of high surface productivity and export production. Biological oxygen consumption falls off rapidly with depth, decreasing by a factor of 10–50 between 100 and 1,000 m (Feely et al., 2004). However, recent studies have revealed the existence of oxygen utilization near the seafloor (Davila et al., 2023; Holzer, 2022; Sulpis et al., 2023).

Large-scale mass and tracer transport across ocean basins is related to the Meridional Overturning Circulation (MOC). The upper cell of the MOC can be traced from the northern North Atlantic, where deep water formation occurs, and it ventilates the upper 2 km of the Atlantic Ocean. A deeper overturning cell, the lower cell, originates around Antarctica and supplies bottom water to the abyssal ocean (Buckley & Marshall, 2015; Rintoul, 2000). By means of the large-scale MOC, the surface water properties along with heat, oxygen, carbon, and nutrients are injected into the ocean interior at high latitudes and distributed from their formation regions throughout the ocean basins (Talley et al., 2003). Due to mass conservation, this relatively slow flow of water masses away from their formation regions must be balanced by a return flow along different pathways. As the result, net oxygen supply to tropical and subtropical regions occurs because poleward flowing water masses carry low-oxygen waters and the compensating equatorward flow transports well oxygenated waters.

Components of the MOC which transit through high-latitude oceans ventilate about two-thirds of the volume of the global ocean interior (below the mixed layer) and up to 80% of the deep ocean below 1,500 m (Khatiwala et al., 2012). Ocean ventilation of interior waters can be achieved by means of different processes spanning all scales of ocean circulation. Some of these processes that are particularly important are the mass flux across the winter mixed layer base (i.e., subduction), interior turbulent mixing, and advection by local to regional circulation. The interplay between the different processes and their relative importance modulates the ocean ventilation and its temporal variability.

Since ongoing global warming adds heat to the upper ocean, oxygen solubility is expected to decrease and overall ocean stratification is expected to increase (Bronselaer et al., 2020; Sarmiento et al., 1998). Increased stratification is associated with less efficient mixing. Thus, reduced ventilation and an older ocean interior is expected under global warming (Gnanadesikan et al., 2007). Previous studies have pointed to reduced ventilation, driven by an increased stratification, as a major cause of ongoing ocean deoxygenation (Breitburg et al., 2018; Gnanadesikan et al., 2007; Helm et al., 2011; Schmidtko et al., 2017). Moreover, qualitative and quantitative understanding of the patterns of oxygen subduction have been described by Portela, Kolodziejczyk, Maes, et al. (2020) but the interplay of the different mechanisms influencing the oxygen content and its transport by the ocean currents is still poorly understood. Hence, the goal of this study is to describe the meridional oxygen transport by different branches of ocean circulation and estimate the AOU along its meridional path in each ocean basin. Our study provides a new framework for future studies of the variability of meridional pathways of oxygen in a warming ocean. Better constraining these pathways is key to better understand regional oxygen variability, its drivers, and trends (Buchanan & Tagliabue, 2021).

2. Methods

2.1. The Model

The simulation used for this study was produced by Mercator-Ocean in the framework of the ERA-CLIM2 project (Buizza et al., 2018). It is an ocean multi-year hindcast simulation of the 20th and early 21st centuries forced by the atmospheric fluxes of the coupled climate reanalysis CERA-20C (Laloyaux et al., 2018). The dynamical ocean, sea-ice (LIM3 model, Rousset et al. (2015)) and biogeochemical components were run together within the ocean model NEMO ("Nucleus for European Modeling of the Ocean") version 3.6 (online coupling). There is no data assimilation in this simulation. The biogeochemical component is based on the PISCES (https://www.pisces-community.org) model (Aumont et al., 2015) that is a model of intermediate complexity. PISCES lies in between a simple Nutrient-Phytoplankton-Zooplankton-Detritus model (NPZD, e.g. a model based only on one nutrient, most likely nitrogen, and with one compartment of phytoplankton, zooplankton and detritus as used in Fasham et al. (1990)) and a complex biogeochemical model aiming to resolve the full complexity of the ecosystem structure (e.g., the DARWIN model with about 80 state variables (Follows et al., 2007),). PISCES has

been used in a variety of studies dealing with oxygen cycles at global and regional scales (e.g., Bopp et al. (2013); Resplandy et al. (2012); Buchanan and Tagliabue (2021)). It has 24 prognostic variables and simulates biogeochemical cycles of oxygen, carbon and the main five nutrients (nitrate, ammonium, phosphate, silicic acid and iron) controlling the growth of two phytoplankton functional groups (i.e., nanophytoplankton and diatoms). Nutrients are supplied to the ocean via three different external sources (climatologies): atmospheric deposition (Fe, Si, N and P), rivers (N, P, Si, Fe, DIC, Alkalinity), and sediments (Fe). The biogeochemical and sea-ice model are coupled through the sea-ice fraction parameter, and air-sea gas exchanges occur only in ice-free regions.

The horizontal grid is the standard "Orca" tri-polar grid at 1° resolution (362 × 292 grid points). The three poles are located over Antarctica, Central Asia and North Canada. 1° corresponds roughly to 110 km of horizontal resolution at the equator. The vertical grid has 75 levels, with a resolution of 1 m near the surface and 200 m in the deep ocean. The simulation protocol is as follows: the run starts in 1870 from a restart of a 100-year climatological simulation using exactly the same code version, then a spin-up of 30 years is forced by a CERA-20C daily climatology. The interannual simulation then starts in 1900. The dataset used to perform the computations of this study is available on the Mercator-Ocean FTP server (ftp://ftp.mercator-ocean.fr/download/eraclim2). This dataset includes a MAT-LAB file with monthly means of DO and the physical variables needed to reproduce the results presented here.

In this study we are using previously existing model outputs and there is no control run available. We have identified some model drift during the early stages of the simulation from 1900 until around 1920 (not shown). For our time-mean analysis, we have used outputs from 1950 on-wards in order to minimize the influence of the initial model adjustment since we cannot estimate the model drift. We have computed the difference between the oxygen concentration in the upper 1,000 m of the water column in 2009 compared to 1970. The oxygen inventory drops by 0.6%. This falls near the lower bound, but within the range estimated in the Intergovernmental Panel on Climate Change (IPCC) report (IPCC, 2022), which is 0.5%–3.3% (see their Table 5.2). In the 0–100 m layer, we obtain a drop of −0.22% between 1970 and 2009. This is again near the lower bound but within IPCC estimates (0.2%–2.1%).

Although the temporal DO change obtained from the model matches the ranges reported by the Intergovernmental Panel on Climate Change (IPCC), this study focuses in the mean state of the global meridional DO transport alone. Therefore, we have compared the time and zonal mean DO concentration computed from the mean climatology of the World Ocean Atlas, 2018 (WOA18, https://www.ncei.noaa.gov/access/world-ocean-atlas-2018/) (Garcia et al., 2019) at 1° resolution, to the NEMO-PISCES model outputs (Figure 1). Model outputs between 1950 and 2009 have been used in order to match the period where most DO observations used in WOA18 were made (see Garcia et al. (2019) for observational bottle data distribution). The model successfully reproduced the mean large-scale features of the DO field. While the model reproduces reasonably well the mean DO in the Indo-Pacific basin, low oxygen waters in the deep Atlantic extend further northward in the NEMO model than in the observations (Figure 3i), this might be related to poor representation of NADW in the model. To get further insight on the source of the model biases, we have calculated the global meridional means of O^{sat}, AOU and the stratification (as the Brünt Väisäla frequency, N^2) both, from the model and from WOA18 (Figure S1 in Supporting Information S1). The model reproduces well the temperature field (and therefore, $Osat$) and the stratification. However, it overestimates the AOU in most of the ocean below 1,000 m since it underestimates the mean DO field (Figure 1g). Our results suggest that the main water masses are generally well represented in the model, while the strongest biases are found in the northern North Atlantic. This is an important region of deep convection and deep water formation (e.g., NADW), both processes are typically difficult to resolve in ocean models (Heuzé, 2017).

In order to check that our model reproduces both the DO distribution and the observed meridional overturning circulation well, we have compared the mean streamfunction in latitude-depth coordinates (Ψ_z) (Figure S2) as obtained from our model simulation with previous model-based studies. Our global streamfunction is in very good agreement with the study of Döös et al. (2012) and Aldama-Campino et al. (2020) (using a different NEMO simulation) both in magnitude and structure. It is also in agreement with the work of Zika et al. (2012) (using the Geophysical Fluid Dynamics Laboratory (GFDL) Modular Ocean Model version 2.2). The streamfunction in Figure S2c also compares well with a data-based streamfunction in the Atlantic Ocean (Talley et al., 2003). Both, exhibit similar vertical and meridional distribution of the 4-Sv contour, as well as similar maximum magnitude (18 Sv in Talley et al. (2003), and around 15 Sv in this study and in Aldama-Campino et al. (2020)). The model validation gives us some confidence in the fidelity of the model-based diagnostics presented here, such as the oxygen-latitude streamfunction, which would not be possible from in-situ data.
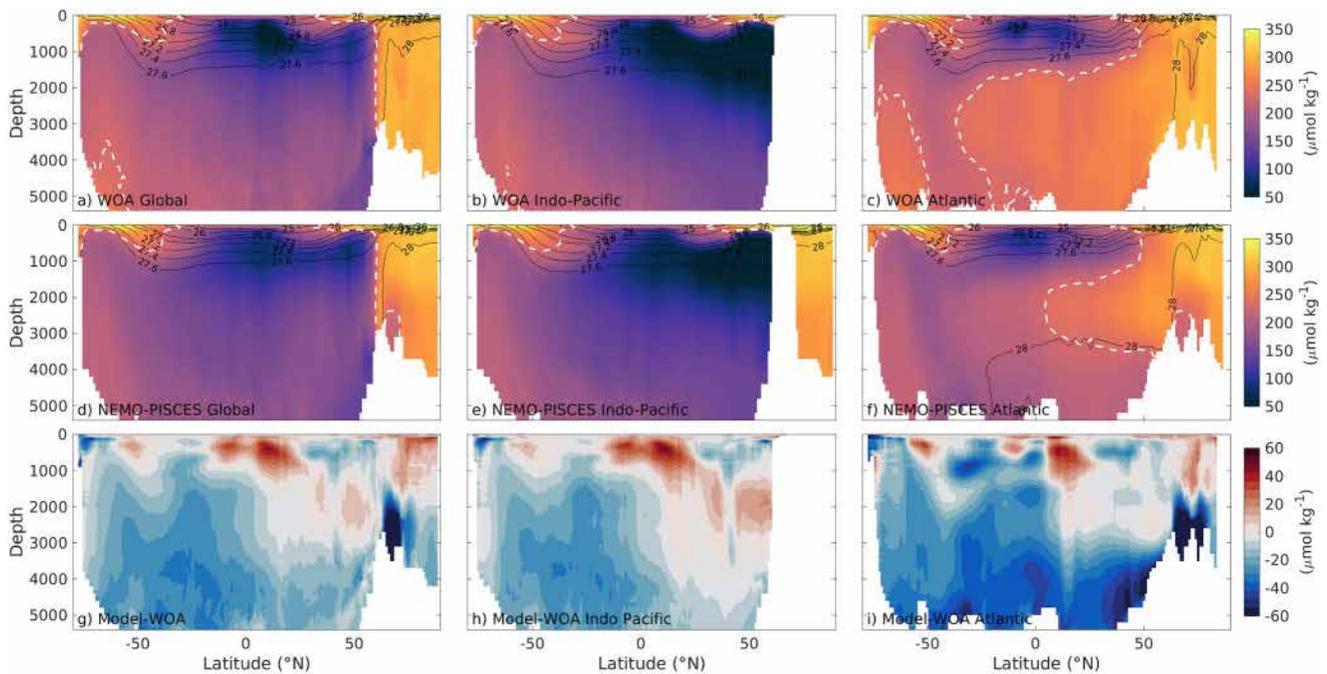
Figure 1. Mean, zonally averaged, DO concentration as provided by (upper row) observations from the World Ocean Atlas, 2018 (WOA18) (middle row) the NEMO-PISCES model and (bottom row) their difference (model minus WOA18) for (a) and (d) the global ocean, (b) and (e) the Indo-Pacific Ocean and (c) and (f) the Atlantic Ocean. Black contours show the isopycnals and the dashed white line highlights the oxypleth of 230 μmol kg^{-1} for reference.

3. Oxygen Streamfunction

We aim to quantify the global meridional oxygen transport in the ocean and its link with the formation and circulation of the main water masses. To this end, we have computed the meridional overturning streamfunction in the classical latitude-depth coordinates (Ψ_z) but also in latitude-oxygen coordinates (Ψ_{O_2}). Since we are mapping the meridional transport into oxygen classes, we track the full range of oxygen concentrations at which the meridional exchange of seawater takes place.

The oxygen streamfunction is defined as the volume (or mass) transport in terms of latitude and DO (following the analogous description of (Ferrari & Ferreira, 2011) for the latitude-temperature streamfunction). The mass transport in DO layers can also be expressed in terms of the DO transport by ocean circulation, both points of view are equivalent. By projecting the flow into the oxygen tracer coordinate, we are also considering the biogeochemical cycle of seawater in DO and latitude space rather than only the physical circulation. Here, DO is not intended to be used as a vertical coordinate but for describing the meridional transport of DO by the various branches of the MOC (i.e., analogous to the application of the temperature-latitude streamfunction by Ferrari and Ferreira (2011)). In this sense, only waters that change oxygen concentration along closed overturning cells (closed contours of the streamfunction) contribute to the meridional DO transport. In contrast, waters that flow poleward and return equatorward at the same oxygen concentration, do not contribute any net meridional oxygen exchange. This novel diagnostic is useful to analyze and quantify the global ocean conversion rate between well oxygenated waters in high latitudes and less oxygenated waters in the tropical oceans.

Our approach of computing Ψ_{O_2} follows the procedure described in previous studies with streamfunctions in coordinates other than latitude-depth. These include cases where depth was substituted for density, which is monotonically increasing with depth (Döös & Webb, 1994), or temperature, which is only notionally monotonic at low to mid-latitudes (Ferrari & Ferreira, 2011; Holmes, Zika, et al., 2019). Others have exploited coordinates which, like oxygen, are clearly non-monotonically increasing with depth, such as latitude-salinity (Ballarotta et al., 2014; Bladwell et al., 2021) and latitude-carbon (Aldama-Campino et al., 2020) and even where both coordinates are time variable tracers such as temperature-salinity (Döös et al., 2012; Zika et al., 2012) or density-carbon (Groeskamp et al., 2016). However, to the best of our knowledge, this type of streamfunction has never been used as a diagnostic to study the global oxygen transport linked to the overturning circulation.

The classical meridional overturning streamfunction (Ψ_z) is assessed for every depth level (z) below a given depth (i.e., the sea surface) and for each time step ($t = 1$ month) by integrating the meridional velocity ($v(\psi, \phi, z, t)$) zonally (with longitude $\psi_1 < \psi < \psi_2$ that varies in each ocean basin, and being $\psi_1 = 0$ and $\psi_2 = 2\pi$ for the global streamfunction) for each latitude (ϕ):

$$\Psi_z(\phi^*, z^*, t) = \int_0^{2\pi} \int_{z < z^*} v(\psi, \phi^*, z, t) \, dz \, d\psi \qquad (1)$$

Similarly, Ψ_{O_2} can be expressed as:

$$\Psi_{O_2}(\phi^*, O_2^*, t) = \int_0^{2\pi} \int_{O_2 < O_2^*} v(\psi, \phi^*, z, t) \, dz \, d\psi \qquad (2)$$

where the symbol (*) denotes the discrete classes of the given variables. Thus, following Equation 1, Ψ_z represents the total meridional volume transport below a given depth class (z^*), at a given latitude (ϕ^*). Similarly, Equation 2 represents the total meridional volume transport below a given discrete DO surface $\left(O_2^*\right)$ at a given latitude (ϕ^*).

Ψ_{O_2} allows identification of the meridional DO pathways once it is injected into the ocean interior and, moreover, it allows description of the DO changes along the meridional water-mass journey. Note here that if a surface of constant DO changes with time (i.e., the ocean is not steady) then, Ψ_{O_2} represents the combined effect of the flow through the given oxygen surface plus the surface displacement (Zika, Sijp, et al., 2013).

To investigate the DO changes due to biological respiration and mixing between water masses of different DO content (AOU) along the meridional water-mass pathway, the same analysis was performed for O_2^{sat} following Equation 2. The solubility pump is the mechanism by which oxygen enters the deep ocean via sites of convection and deep water formation. This typically occurs at high latitudes, where cooler surface temperatures increase oxygen solubility. From these locations of oxygen injection into the ocean interior, the oxygen concentration decreases as the waters get older and mix with less oxygenated waters along their path. Therefore, the comparison between the streamfunction in DO, and O_2^{sat} coordinates provides more insight about the processes involved in the MOC-related oxygen variability. For a more detailed formulation of the generalized streamfunction to any coordinate see Zika et al. (2012) and Aldama-Campino et al. (2020).

A schematic of Ψ_{O_2} and the explanation on how to read the DO changes along its circulation path is provided in Figure 2. The link between Ψ_{O_2} and Ψ_z is not trivial due to the non-monotonic vertical DO distribution. However, some equivalences can be made by taking into account the following features in Figure 2: (a) vertical displacements in Ψ_{O_2} correspond with flow up or down DO gradients (b) horizontal displacements in Ψ_{O_2} represent meridional transport along constant DO surfaces, that is, no net DO transport. In contrast, $\Psi_{O_2^{sat}}$ reflects the meridional changes in oxygen solubility, which is a strong function of temperature. Consequently, horizontal displacements in $\Psi_{O_2^{sat}}$ coordinates represent mainly adiabatic transport (i.e., approximately along isotherms), while vertical displacements indicate diabatic circulation (i.e., across isotherms). This means that (c) Ψ_{O_2} slopes only imply mixing between waters with different oxygen concentration, or oxygen consumption (AOU) if they differ from $\Psi_{O_2^{sat}}$ slopes. In regions where both curves are nearly parallel (equal slopes), even if they are not equal (if an offset exists), the meridional DO change is due to solubility changes, that is, mixed-layer meridional temperature differences that affect $\Psi_{O_2^{sat}}$ and Ψ_{O_2} in the same way in the absence of mixing. Thus, (iv) circulation within the mixed layer, where seawater is nearly saturated in oxygen, can be identified by the overlapping of Ψ_{O_2} and $\Psi_{O_2^{sat}}$.

In our model simulation, purely horizontal Ψ_{O_2} cells (i.e., meridional DO transport with zero change in oxygen concentration) are not observed. This agrees with what is expected in the real ocean, where DO is consumed and mixed along its journey while transported away from the water-mass formation sites. In the large scale, within the mixed layer, oxygen is near saturation as water re-saturates constantly due to air-sea exchanges. However, the meridional temperature gradient implies changes in solubility and, therefore, in the oxygen concentration. In this case, the slopes of Ψ_{O_2} and $\Psi_{O_2^{sat}}$ will be mostly equal because the DO changes are purely driven by solubility
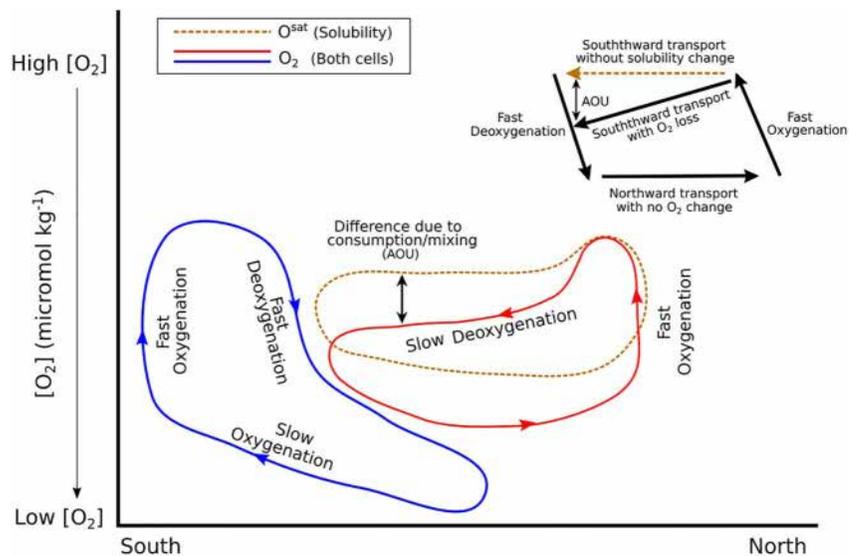
Figure 2. Schematic of Ψ_{O_2} and $\Psi_{O_2^{sat}}$ for the southern (blue) and northern (red) cells of the meridional oxygen circulation. Displacements along the *y*-axis in this framework represent local, rapid (de)oxygenation, while nearly horizontal patterns along the *x*-axis evidence long journeys of the water masses with little mixing and/or biological oxygen consumption/production.

changes. In the ocean interior, where the water masses DO is below saturation, oxygen decreases due to progressive biological consumption, and any water-mass transport implies some degree of oxygen depletion regarding its saturation concentration. In this case, the slope of Ψ_{O_2} will decrease faster than that of $\Psi_{O_2^{sat}}$. The opposite occurs when the MOC transits poleward, and the oxygen-depleted waters mix with "younger" more oxygenated waters. In this case, the slope of Ψ_{O_2} will increase faster than that of $\Psi_{O_2^{sat}}$. It is precisely the difference between the slope of Ψ_{O_2} and $\Psi_{O_2^{sat}}$ that determines the relative contribution of AOU to the total meridional DO change. Although it is reasonably accurate in the large scale and mean state processes, one limitation of this approach is that it does not take into account the disequilibrium of the surface DO with respect to the atmospheric oxygen concentration. In low-latitudes, the surface ocean is slightly supersaturated in oxygen due to photosynthesis and sluggish ventilation. In contrast, in high latitudes, and particularly in strong convection regions, the mixed-layer waters can be undersaturated in oxygen due to rapid heat loss and strong convective mixing of large volumes of DO-depleted deep waters to the surface (Frölicher et al., 2020; Ito et al., 2004). This high-latitude disequilibrium can have an impact in our AOU estimation and will be discussed in the next section.

4. Results and Discussion

4.1. Mean Meridional Oxygen Distribution and Overturning Circulation

The mean meridional oxygen distribution obtained from the model outputs over the period 1950–2009 (Figures 3a–3c) shows major features previously reported in the literature. Since DO solubility increases at low temperatures, the most oxygenated waters of the global ocean are those of high latitudes (as reflected by Figure 3 d-e). However, oceanic DO distribution results from the balance between water-mass age, biological production and consumption and circulation. Despite the Atlantic Ocean being warmer than the Indo-Pacific and, therefore, showing lower O_2^{sat} (Figures 3d–3f), absolute DO maxima are found in the North Atlantic, the Nordic Seas and the Arctic Ocean (Figures 3a–3c). This is because, high latitudes are also important ventilation hotspots (Morrison et al., 2022; Portela, Kolodziejczyk, Maes, et al., 2020) where younger and more oxygenated waters are present. A model's ability to accurately reproduce all the aforementioned processes will influence its ability to reproduce ocean oxygen content.

In the Subpolar North Atlantic and the Nordic Seas, during winter deep convection, North Atlantic Deep Water (NADW) is injected into the intermediate/deep ocean (1,000–3,000 m depth) and transported southward carrying well oxygenated waters. The Atlantic Meridional Overturning Circulation (AMOC) is evidenced by the main
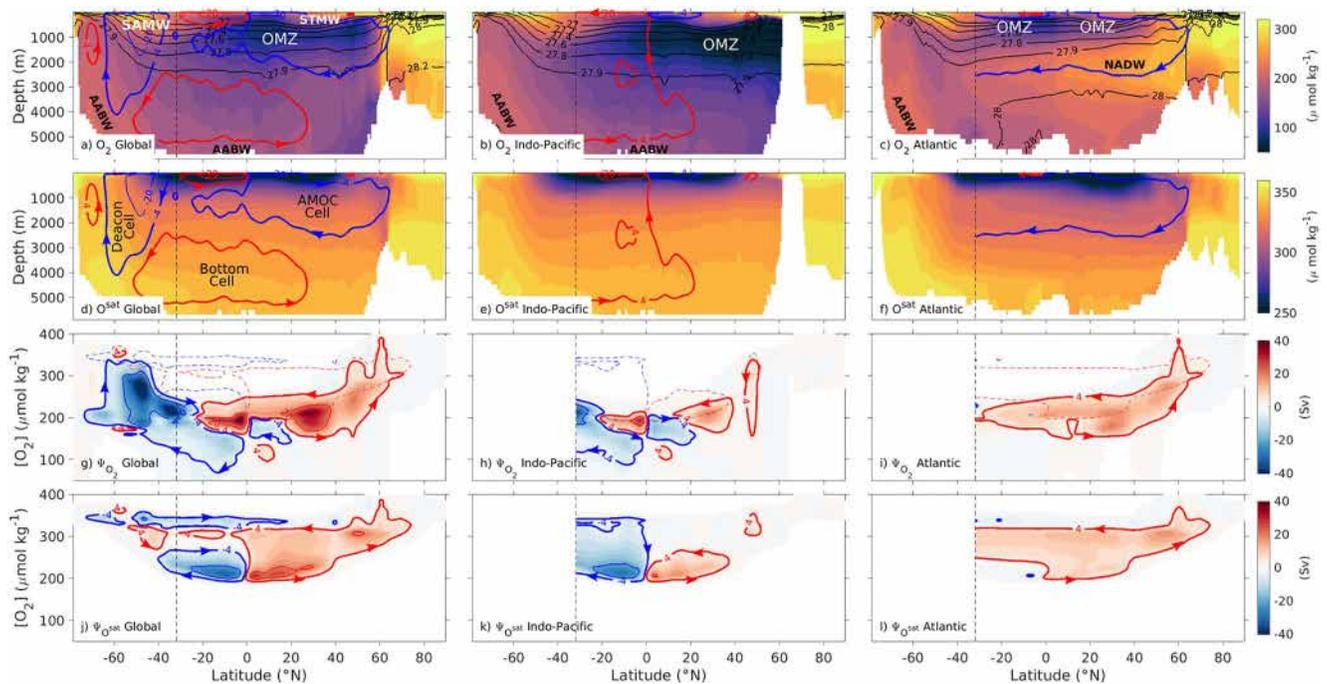
Figure 3. Mean value over the period 1950–2009 of (a)–(c) meridional oxygen concentration (colormap) and Ψ_z (contours), (d)–(f) meridional O_2^{sat} and Ψ_z (contours), (g)–(i) Ψ_{O_2} and (j–l) $\Psi_{O_2^{sat}}$. Each column represents a different region: (a, d, g, j) global ocean (b, e, h, k), Indo-Pacific basin and (c, f, i, l) Atlantic basin. The blue (red) cells spin clockwise (counterclockwise). The ±4 Sv streamlines are highlighted with thick lines and thin lines represent ±20 Sv. In panels (g)–(i) the ±4 Sv streamlines of $\Psi_{O_2^{sat}}$ are superposed as dashed lines. Ψ_{O_2}, $\Psi_{O_2^{sat}}$ and Ψ_z in the Southern Ocean are only represented globally. The Southern Ocean northern limit as defined in this study is marked with a straight dashed line at latitude 32°S. The delimitation of the ocean basins was made by applying the mask provided in ftp://ftp.mercator-ocean.fr/download/eraclim2.

meridional cell in the Atlantic Ocean that spans almost the entire basin between the northern subpolar latitudes and the Southern Ocean (Figures 3c and 3f). When the AMOC reaches the Southern Ocean, oxygen-rich NADW merges with the Circumpolar Deep Water (CDW), mainly found in the Indo-Pacific basin, and upwells within the Antarctic Circumpolar Current (ACC) (Lumpkin & Speer, 2007; Speer et al., 2000; Tamsitt et al., 2017), (Figure 3a) where waters replenish in DO.

In the Southern hemisphere, there are two DO maxima over the water column (Figure 3a) that correspond to the two branches of the Southern Ocean overturning circulation (Morrison et al., 2022). The Lower (L)CDW upwells near Antarctica (Marshall & Speer, 2012), loses buoyancy due to brine rejection (Hasumi & Suginohara, 1995; Jacobs, 2004) and sinks to form Antarctic Bottom Water (AABW) (Deacon, 1937; Speer et al., 2000). This water mass slowly ventilates the ocean abyss by carrying oxygenated waters northward (Figures 3a and 3d, and Rintoul (2000)). The upper (U)CDW upwells within the ACC belt, and it is advected northward by the Ekman transport. Then, it gains buoyancy and forms Sub-Antarctic Mode Water (SAMW) in the upper layers. SAMW is subsequently subducted into the ocean interior during late winter and advected northwestward at intermediate depths (up to 1,000 m) (Hanawa & Talley, 2001). This SAMW, that has a noticeably high DO signature in all basins (Figures 3a–3c), is the main source of oxygen into intermediate depths in the Southern Hemisphere (Portela, Kolodziejczyk, Maes, et al., 2020) (Figures 3a–3c). A similar process takes place within the subtropical gyres of both hemispheres in the so-called subtropical cells (Oschlies et al., 2018). There, the convective injection (Kolodziejczyk et al., 2015) and the wind-driven subduction of Subtropical Mode Waters (STMW) bring surface oxygenated waters into the ocean interior between 20°N and 40°N (Portela, Kolodziejczyk, Maes, et al., 2020). The Oxygen Minimum Zones (OMZ), located at the so-called "shadow zones" of the subtropical cells (Luyten et al., 1983), are the result of weak ventilation and high biological oxygen consumption rates in these regions (Brandt et al., 2015; Oschlies et al., 2018). However, recent studies suggest that the role of oxygen consumption might be less important than previously thought, and that the transport of low-oxygen waters seems to be the dominant driver of the existence of the OMZs (Davila et al., 2023; Holzer, 2022). These OMZs are larger and more intense in the Indo-Pacific basin due to the absence of important ventilation there. The OMZs are visible by

their low oxygen concentration in Figures 3a–3c but they are not represented in Figures 3g–3i because the meridional transport is too weak.

The meridional DO distribution in the global ocean is the result of different ventilation mechanisms. Ocean ventilation by subduction is well identified in regions of mode water formation (Portela, Kolodziejczyk, Maes, et al., 2020). However, the interior oxygen spreading associated with meridional circulation is less documented. In the following, we will focus on the role of the meridional overturning circulation in the oxygen transport and on the drivers of the simulated spatial oxygen variability.

4.2. Oxygen-Latitude Streamfunction

When projected in latitude-DO coordinates, the global meridional DO circulation (Figure 3g) is reduced to only two extensive and asymmetric cells of opposing sign that span each an entire hemisphere. Hereinafter, they will be referred to as the Northern and the Southern cells. Since the Atlantic and Indo-Pacific sectors of the Southern Ocean are connected through Drake's Passage and south of Africa, the flow can not be described by a streamfunction where there is a strong zonal flow between ocean basins. This limit, an ad hoc choice, is set to be 32°S (the tip of the African continent) and, therefore, no streamfunction is shown south of this latitude for the individual basins (Figure 3, middle and right columns). The maximum meridional transport by the Southern cell reaches 48 Sv in the Southern Ocean, at 48.3°S and DO of 270 µmol kg^{-1}, while the global maximum of the Northern cell is 38.6 Sv at 3.4°S and DO of 193 µmol kg^{-1}.

4.2.1. The Northern Cell

The Northern Cell of Ψ_{O_2} in the global ocean (Figure 3g) is mostly explained by the AMOC in the Atlantic basin (Figure 3i), with maximum transport of 19.4 Sv occurring at 29.6°N and with DO = 180 µmol kg^{-1}. NADW forms in the northern North Atlantic and the Nordic Seas and is ventilated into the deep ocean around 60°N (Figure 3i). NADW is saturated (even supersaturated, see Feucher et al. (2022)) in oxygen as revealed by the overlapping of Ψ_{O_2} and $\Psi_{O_2^{sat}}$ (Figure 3j), but it crosses an DO gradient and strongly deoxygenates along its transit from 60° to 40°N. During this transit, it loses 114 µmol kg^{-1} in 20° of latitude (-5.7 µmol kg^{-1} per degree of latitude). From 40°N the NADW loses DO slowly along its nearly adiabatic southward transport; it loses only 40 µmol kg^{-1} along 70° of latitude (-0.6 µmol kg^{-1} per degree of latitude (Figure 3f)). The returning point of the AMOC cell in Ψ_{O_2} occurs at 30°S in the Atlantic Ocean (Figure 3i), just before it encounters the Southern Ocean. At this point, the Northern cell has lost 45% of its initial oxygen concentration; 15% of which can be attributed to solubility effects and the remainder 30% to AOU-related processes. These percentages do not take into account the air-sea disequilibrium, which could slightly reduce the role of the AOU. Nevertheless, in the North Atlantic our streamfunctions show mainly a supersaturation of the waters formed in deep convection regions (around 60° N). This is in agreement with the findings of Feucher et al. (2022), who found DO supersaturated waters in the Labrador Sea over certain periods. On its way back North near the surface, DO loss occurs until 10°N, as the returning branch of the AMOC crosses oxygen-depleted tropical waters. This is followed by a DO gain while the tropical water masses transit toward higher latitudes and mix with more oxygenated waters. The DO gain is progressive from 10°N to 40°N, and abrupt from 40°N to 60°N, at the approximate location of the front separating the Gulf Stream and North Atlantic drift. Finally, these waters undergo deep convection and oxygenation again at the ventilation region around 60°N in the North Atlantic basin and the Nordic Seas.

The Northern Cell, as represented in the global zonal average, integrates some additional features besides the AMOC. Between 0° and 20°N, the small clockwise cell combines the northward circulation of AABW, with the North Pacific tropical cell. Furthermore, in the Indo-Pacific basin, specifically in the Pacific Ocean (not shown) there is a shallow clockwise cell centered at 50°N (Figure 3h) that is related to the North Pacific Subpolar Gyre. Its signature is weak in Ψ_z, but it spans a large DO range in Ψ_{O_2}. However, this North Pacific cell is isolated from any other overturning circulation cell, and does not play a significant role in the global meridional oxygen transport.

4.2.2. The Southern Cell

The clockwise Southern Cell of the global oxygen streamfunction is dominated by the circulation in the Indo-Pacific basin, and it will be described in these terms. This is mainly due to the largest volume occupied by these two basins in the Southern Hemisphere in comparison with that of the narrower Atlantic basin.

In the Southern Ocean, the Southern Cell shows the intense upwelling of old, relatively deoxygenated waters all the way to the surface at $\sim$ 65°S, where oxygen concentration increases from $\sim$180–335 μmol kg^{-1}. This feature in Ψ_{O_2} is coincident with the Deacon cell in Ψ_z (the southernmost clockwise cell in Figure 3a) that represents the zonal and time mean upwelling poleward of the zonal surface-wind maximum and downwelling equatorward of this maximum in the Southern Ocean (Marshall & Speer, 2012). The Deacon cell does not represent the true exchanges of water masses in the Southern Ocean since the zonal and time average do not capture standing and transient eddy processes, which may transport tracers both meridionally and vertically (Zika, Sommer, et al., 2013). However, Ψ_{O_2} shows DO resaturation in the ocean surface that is consistent with the strong upwelling and DO replenishment of old waters. At high latitudes (60–70°S), the formation and downwelling of AABW is represented by Ψ_{O_2} with DO around 200 μmol kg^{-1}. Northward of the upwelling region ($\sim$60°S), the Southern Cell transports surface oxygen saturated waters northward at nearly constant oxygen concentration between 60°S to $\sim$45°S, where the subduction of SAMW and AAIW occurs and the oxygen concentration decreases quickly at intermediate depths (Figures 3a and 3g). From 45°S until the Equator, Ψ_{O_2} shows the combined northward transport and DO loss of the bottom and the subtropical Ψ_z cells (Figure 3a). This is also visible from $\Psi_{O_2^{sat}}$ where the bottom cell appears as a well oxygenated clockwise circulation and the subtropical cell exhibits the lowest oxygen saturation between 40°S and the Equator (Figure 3j). Between 20°S and the Equator the Southern and Northern cells share latitude range but carry waters with different oxygen concentration in different basins (Figures 3g–3i). For the Southern Cell, the northward transport of waters with oxygen concentration from around 200 μmol kg^{-1} mainly represents the spreading of AABW into the abyss (Figures 3b and 3h), while for the Northern Cell, it is linked to the returning branch of the AMOC (Figures 3c and 3i).

The Southern Cell turns southward at the Equator and, due to the proximity of the Pacific OMZs, it continues losing oxygen until 15°S where it achieves the absolute global minimum DO class (70 μmol kg^{-1}) that is represented by Ψ_{O_2} (Figures 3b and 3h). At this point, the Southern Cell has lost 76% of the oxygen concentration it had at its origin at $\sim$60°S. The pronounced slope of Ψ_{O_2} in comparison with $\Psi_{O_2^{sat}}$ indicates important contribution of mixing/consumption processes to the oxygen decrease. From its oxygen minimum, the Southern Cell gains around 110 μmol kg^{-1} in oxygen concentration along its poleward path from 15°S to 50°S. This is mainly explained by mixing, along the southward journey, with relatively DO-rich waters which are younger (more recently formed) and had a higher DO at the moment of their formation (due to the higher O_2^{sat} in cold waters). At 60°S the intense upwelling results in DO resaturation at the surface (Figures 3a and 3g) that closes the DO overturning cell.

4.3. Oxygen Saturation Streamfunction

The $\Psi_{O_2^{sat}}$ (Figures 3j–3l) is closely related to the meridional overturning circulation in latitude-temperature coordinates, since O_2^{sat} mainly depends on seawater temperature (Ballarotta et al., 2014; Döös et al., 2012; Ferrari & Ferreira, 2011; Holmes, Lavergne, et al., 2019; Zika et al., 2012). In the Atlantic basin, the AMOC cell has a similar shape in $\Psi_{O_2^{sat}}$ and Ψ_{O_2} (Figure 3, i,l) which reveals the relatively weak AOU during its journey. The strongest DO loss occurs just after the injection of well oxygenated waters at 60°N (Labrador and Irminguer seas). At this point, besides the decrease in oxygen solubility, we observe an abrupt divergence of the 4 Sv $\Psi_{O_2^{sat}}$ and Ψ_{O_2} contours (Figure 3i). This separation between both streamfunctions implies DO loss is not due to solubility loss and can be attributed to strong meridional AOU occurring between 60°N and 40°N. Over the AMOC's southward path, the difference between Ψ_{O_2} and $\Psi_{O_2^{sat}}$ reveals that the Northern cell transports oxygen 30%–40% below saturation. Moreover, the difference in both streamfunction's slopes, and the fact that the $\Psi_{O_2^{sat}}$ slope is nearly zero, indicates that the DO loss is due to AOU. In contrast, the northward returning path of the AMOC cell occurs near the surface, and it is mainly solubility-driven, that is, the slopes of both streamfunctions are similar (see Figure 2). From 40 to 70°N the oxygen concentration of the transported waters increases poleward due, in part, to the increase in O_2^{sat} with latitude. However, the ascendent slope of Ψ_{O_2} is steeper than that of $\Psi_{O_2^{sat}}$, which indicates an increase in AOU likely due to mixing with more oxygenated waters poleward. Ultimately, DO increases due to deep convection and oxygen resaturation in the Northern North Atlantic.

In the Southern Hemisphere $\Psi_{O_2^{sat}}$ exhibits two cells; the bottom cell with mean O_2^{sat} around 350 μmol kg^{-1}, and the subtropical cell with O_2^{sat} around 250 μmol kg^{-1} (Figure 3j). Between these two clockwise cells, there is an anticlockwise circulation of NADW/CDW coming into the Southern Ocean from the North Atlantic (Figures 3j and 3l). Interestingly, these two cells are merged in Ψ_{O_2}, which differs from the shape of $\Psi_{O_2^{sat}}$. This is the result of

the bi-modal vertical structure of the oxygen concentration, and indicates that the meridional oxygen variability is dominated by dynamical and biogeochemical processes other than solubility changes. This suggests that, unlike the AMOC, whose deep southward branch is close to adiabatic in the Northern Hemisphere, the Southern Cell is highly diabatic and the oxygen transport in the Indo-Pacific basins is dominated by mixing/consumption (AOU).

4.4. Meridional Isopycnal Oxygen Transport

Since the oxygen streamfunction hides the three-dimensional structure of the oxygen circulation, we seek to understand how oxygen circulates on isopycnals and the link between the main Ψ_{O_2} overturning cells described before.

Following Zika, Sijp, et al. (2013), for any variable $C(x, y, z, t)$ a distribution function (M) can be computed to describe the transport in any direction over a range of values of C. The tracer C can be any passive or active tracer

$$M_C^y(C^*, y) = \frac{1}{\Delta t}\int_t^{t+\Delta t}\int_0^{2\pi}\int_{-z}^0 \delta(C - C^*)\, v\; d\psi dz dt \qquad (3)$$

where v is the meridional velocity, δ is the Dirac delta function and the term $\delta(C - C^*)$ represents the discretization of the domain in tracer classes indicated by the symbol (*). This equation can be generalized to compute the joint distribution in any two tracer coordinates C_1 and C_2. In the case of this study, C_1 will be potential density (σ_0) and C_2 will be oxygen concentration (O_2). Therefore, the Equation 3 can be expressed as follows:

$$M_{\sigma_0, O_2}^y(\sigma_0, O_2, y) = \frac{1}{\Delta t}\int_t^{t+\Delta t}\int_0^{2\pi}\int_{-z}^0 \delta(\sigma_0^* - \sigma_0)\delta(O_2^* - O_2)\, v\; d\psi dz dt \qquad (4)$$

By using Equation 4, we averaged the meridional volume transport (per unit of oxygen and density) in oxygen-density coordinates across two key latitudes for the global ocean circulation: 32°S, which is the northern limit of the Southern Ocean (Figures 4a–4c), and 55°N in the North Atlantic to account for the oxygen transport by the AMOC near the region of deep water formation (Figure 4d). These latitudes represent regions where large volumes of recently ventilated waters are transported equatorward. Therefore, the meridional transport joint distribution in oxygen-density space provides a more detailed view of the exchange of the main water masses, and their DO content across these boundaries.

In the Southern Ocean, northward and southward isopycnal transport of waters with different oxygen concentration is observed at every isopycnal layer. This represents the zonal variability of the oxygen concentration and transport at 32°S, a feature that is neglected by the streamfunctions due to the zonal average. Globally, the northward flow from the Southern Ocean carries well oxygenated waters at intermediate ($\sigma_0 < 27.6$ kg m^{-3}) and bottom ($\sigma_0 = 28$ kg m^{-3}) layers. The most important intermediate water mass in terms of oxygen concentration is the SAMW (DO between 200 and 260 µmol kg^{-1}, Figures 4a and 4b), while in abyssal layers, the AABW is relatively less oxygenated (DO between 170 and 200 µmol kg^{-1}). Since the net DO flux across the Southern Ocean boundary varies among basins (Figures 4a–4c, insets), the southward currents transport water masses of different origin with different oxygen concentration into the Southern Ocean at deep layers ($27.6 < \sigma_0 < 27.9$ kg m^{-3}) (inset in Figure 4). The main global features of the meridional transport into/from the Southern Ocean are dominated by those in the Indo-Pacific basin (Figure 4b) due to its volumetric preponderance over the Atlantic Ocean. In the Indo-Pacific, the different characteristics of the transport in the Indian and the Pacific basins result in two different branches of DO transport (Figure S3). The equatorward transport of SAMW between 26.8 and 27.2 kg m^{-3} is evidenced by the maximum oxygen concentration that reveals its recent formation. The SAMW exhibits two DO maxima: the most oxygenated Mode Waters are found in the Indian basin (Figure S3a and Figure 4b), with oxygen concentration between 230 and 250 µmol kg^{-1}, while it ranges between 200 and 220 µmol kg^{-1} in the Pacific basin (Figure S3b). Similarly, the southward transport occurs in two branches: the Pacific branch has lower oxygen concentrations than the Indian branch (Figure S3a and S3b in Supporting Information S1, and Figure 4b), especially within the densest layers. At 32°S, the Indian, and the Pacific branches are connected via waters lighter than 26.7 kg m^{-3} (the two branches are joined together) but they are disconnected in denser layers (27.4–27.8 µmol kg^{-1}), indicating different circulation paths and water masses. The waters of tropical origin of all basins have minimal transport per unit density and oxygen, but encompass a wide range of isopycnal layers at low oxygen concentration.
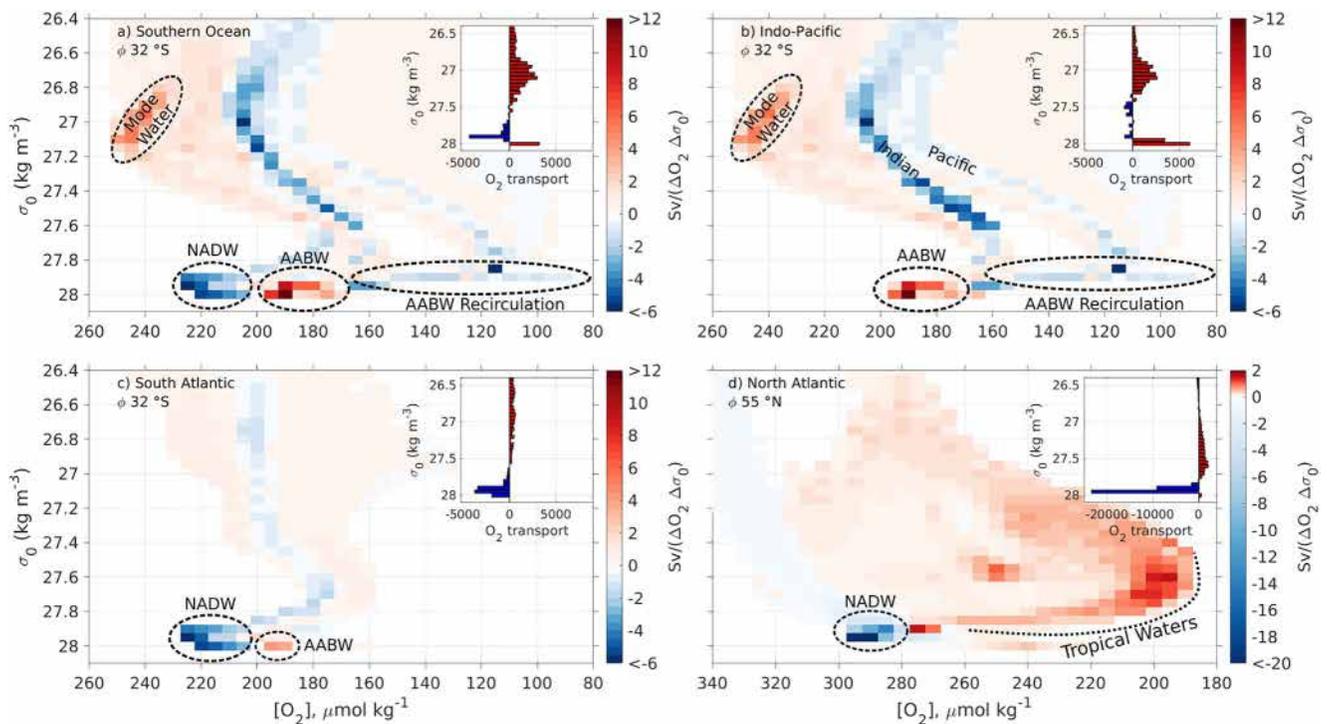
Figure 4. Meridional transport joint distribution in oxygen-density coordinates. Across (a)–(c) 32°S in (a) the whole Southern Ocean, (b) the Indo-Pacific sector and (c) the Atlantic sector (i.e., between 7°W and 59°W). (d) Same as (a)–(c) but for the transport across 55°N, only in the Atlantic sector. The insets show the integrated oxygen transport on each isopycnal layer normalized by oxygen and density units. Blue (red) colors represent poleward (equatorward) transport. The main water masses are labeled in the figure. Note the different scale in positive and negative values in the color bar, and the different x-axis in panel (d).

In deep-to-bottom layers the most oxygenated water (DO around 205–235 µmol kg^{-1}) is the NADW that enters the Southern Ocean from the Atlantic sector on the 27.85–28 kg m^{-3} isopycnals (Figure 4c). On the same isopycnal range, AABW of southern origin spreads northward mainly in the Indo-Pacific sector, with DO between 170 and 195 µmol kg^{-1} (Figure 4b). The most oxygenated AABW is found in the Pacific basin (Figure S3b in Supporting Information S1). Although the NADW core is found around 3,000 m depth, it circulates on the same isopycnals as the AABW, which occupies the ocean bottom at ~5,000 m depth. The resulting balance is a net DO import from the Southern Ocean coming from the Atlantic sector (Figure 4a, inset). In addition, relatively oxygen-poor waters ranging between 80 and 150 µmol kg^{-1} are transported southward on the 28.9 kg m^{-3} isopycnal. This transport can be attributed to the AABW recirculation in the Pacific Ocean.

In the Northern Hemisphere, the meridional isopycnal transport across 55°N in the North Atlantic basin (Figure 4d) provides additional insight on DO transport by the AMOC. The northern North Atlantic is, along with the Southern Ocean, the other main hot-spot for the interior ocean ventilation and DO uptake (Feucher et al., 2022; Portela, Kolodziejczyk, Maes, et al., 2020). The AMOC carries the newly formed and well oxygenated NADW southwards, with DO between 280 and 300 µmol kg^{-1} along the 27.85–27.95 kg m^{-3} isopycnals (Figure 4d). From its ventilation region in the North Atlantic to the latitude where it joins the Southern Ocean, the NADW loses between 60 and 70 µmol kg^{-1} of oxygen concentration (about 25%) and becomes slightly denser (Figure 4c). The remainder of the transport through 55°N is accounted for by the returning branch of the AMOC, whose northward transport of oxygen-poor tropical-origin waters is much weaker than that of the southward branch (Figure 4d).

4.5. Summary and Conclusions

A new oxygen-latitude streamfunction (Ψ_{O_2}) has been used to investigate the global meridional DO transport. Vertical displacements in Ψ_{O_2} correspond with flow up or down oxygen gradients while horizontal displacements represent meridional transport along constant DO surfaces, that is, no net DO transport. This tool has proven to be

useful to reduce the complexity in the representation of the oxygen transport by the MOC. Additionally, the difference in the slopes of Ψ_{O_2} and $\Psi_{O_2^{sat}}$ provides an estimation of the AOU contribution to meridional DO changes.

In the global ocean, oxygen circulates in two main meridional cells. The Northern Cell is explained by the AMOC in the North Atlantic and extends from 60°N to at least 30°S, where part of it joins the ACC in the Southern Ocean. The Southern Cell is dominated by the meridional transport in the Indo-Pacific basin. These cells show some particular features that shed new light on the DO pathways along the water-mass journey around the global ocean, as well as on the driving mechanisms of the meridional oxygen change. In particular:

(i) The Southern Cell contains the lowest oxygen levels in the global ocean (the outer boundary of the Pacific OMZs) while the Northern Cell includes the absolute oxygen maximum, observed in the northern North Atlantic Ocean.

(ii) In the southward-flowing part of the Northern Cell, after a sharp DO gradient driven by strong AOU-derived processes between 55°N and 40°N, the DO transport driven by the AMOC occurs mainly along oxygen surfaces with only gradual DO changes. In contrast, within the Southern Cell, and mainly in the Southern Ocean, the oxygen transport shows strong DO gradients. The latter can be attributed to the merging of the subtropical and bottom Ψ_z cells in the oxygen streamfunction.

(iii) The Northern Cell loses oxygen slowly along the equatorward journey of the NADW at mid-depth. In the North Atlantic it loses 45% of its initial oxygen concentration from its origin to the Ψ_{O_2} AMOC returning point at $\sim$ 30°S, just before it encounters the Southern Ocean (1.7 µmol kg^{-1}/per degree of latitude). About 15% of this DO loss can be attributed to solubility effects, and the remaining 30% to AOU-related processes. On the other hand, the Southern Cell undergoes strong mixing/consumption during its southward journey. It shows abrupt oxygen gradients and it combines different Ψ_z cells that display complex structure in more classical frameworks. The Southern Cell loses 59% of its oxygen on route from its maximum concentration at 65°S to the point where the cell returns near the equator with an overall loss rate of 3.5 µmol kg^{-1}/per degree of latitude. This DO loss reaches 76% if we consider only the journey from the origin to its minimum oxygen concentration at 10°S. This stronger DO loss within the Southern Cell could be partly explained by the longer residence time due to a slower circulation of the large bottom cell of the MOC. The contribution of solubility and AOU to the DO loss during the Southern Cell journey has to be split into the bottom and the subtropical branches.

The analysis of the meridional isopycnal DO transport through the main ventilation regions of the global ocean, that is, the Southern Ocean and the northern North Atlantic, has provided additional information to the meridional oxygen circulation. Overall, the northward-flowing waters from the Southern Ocean supply oxygen at intermediate layers through Mode Water formation, and at bottom layers by the northward spread of relatively oxygenated AABW. In deep layers, the Southern Ocean receives oxygenated waters carried by the AMOC, which drives the most intense DO transport of the global ocean. Well oxygenated NADW leaves its formation region in the northern North Atlantic and is transported southward until it joins the Southern Ocean. From 55°N, near its formation region, to 32°S the northern limit of the Southern Ocean, NADW loses about 60–70 µmol, which represents 25% of its oxygen concentration.

Contrary to the case of carbon (Aldama-Campino et al., 2020), where the solubility pump dominates its pole-to-equator transport, the simulated meridional DO transport in the Southern Hemisphere is controlled, to first order, by the global circulation and mixing processes. This means that the Southern Hemisphere meridional DO distribution greatly differs from what it would be expected by its solubility alone. For instance, AABW has oxygen concentration way below its saturation values. This is likely the result of several concomitant processes. On the one hand, the presence of sea ice in the formation region and the limited residence time of waters at the surface result in the surface waters being likely undersaturated (Ito et al., 2004). On the other hand, the importance of AOU, besides the mentioned disequilibrium at the air-sea interface, suggests the main role of mixing with less oxygenated waters in setting the oxygen concentration of the interior waters. In contrast, in the North Atlantic basin the solubility pump drives the meridional oxygen distribution.

The results of this study provide new insight on the meridional oxygen pathways in the global ocean and suggest that the mechanisms driving oxygen transport along isopycnals are more complex than previously thought. Further investigation involving finer resolution models and biogeochemically driven diagnostics would be of

great interest for addressing the remaining question on the relative role of physics and biogeochemistry on the regulation of long-term spatio-temporal oxygen variability. Moreover, this latitude-oxygen framework can be used in future studies for model evaluation and intercomparison, as well as a diagnostic tool to compare present and future conditions and the impact of the MOC on the oxygen concentration and transport in the global ocean.

Data Availability Statement

The model outputs needed to reproduce the results as well as the MATLAB file with all variables and the main diagnostics used in this study are publicly available in the Mercator-Ocean FTP server (ftp://ftp.mercator-ocean.fr/download/eraclim2), no registration is required. The atmospheric fluxes of the coupled climate reanalysis CERA-20C used as forcing for the model come from (Laloyaux et al., 2018) and can accessed here https://www.ecmwf.int/en/forecasts/dataset/coupled-reanalysis-20th-century. The dynamical ocean, sea-ice (LIM3 model) is presented in Rousset et al. (2015) and can be downloaded from the NEMO web site at this address: https://forge.nemo-ocean.eu/nemo. The WOA18 dataset (Garcia et al., 2019) used for model validation can be accessed in https://www.ncei.noaa.gov/access/world-ocean-atlas-2018/.

References

Aldama-Campino, A., Fransner, F., Ödalen, M., Groeskamp, S., Yool, A., Döös, K., & Nycander, J. (2020). Meridional ocean carbon transport. *Global Biogeochemical Cycles*, *34*(9). https://doi.org/10.1029/2019GB006336

Aumont, O., Ethé, C., Tagliabue, A., Bopp, L., & Gehlen, M. (2015). PISCES-v2: An ocean biogeochemical model for carbon and ecosystem studies. *Geoscientific Model Development*, *8*, 2465–2513. https://doi.org/10.5194/gmd-8-2465-2015

Ballarotta, M., Falahat, S., Brodeau, L., & Döös, K. (2014). On the glacial and interglacial thermohaline circulation and the associated transports of heat and freshwater. *Ocean Science*, *10*(6), 907–921. https://doi.org/10.5194/os-10-907-2014

Bladwell, C., Holmes, R. M., & Zika, J. D. (2021). Internal salt content: A useful framework for understanding the oceanic branch of the water cycle. *Journal of Physical Oceanography*, *4*. https://doi.org/10.1175/jpo-d-20-0212.1

Bopp, L., Resplandy, L., Orr, J. C., Doney, S. C., Dunne, J. P., Gehlen, M., et al. (2013). Multiple stressors of ocean ecosystems in the 21st century: Projections with CMIP5 models. *Biogeosciences*, *10*, 6225–6245. https://doi.org/10.5194/bg-10-6225-2013

Brandt, P., Bange, H. W., Banyte, D., Dengler, M., Didwischus, S. H., Fischer, T., et al. (2015). On the role of circulation and mixing in the ventilation of oxygen minimum zones with a focus on the eastern tropical North Atlantic. *Biogeosciences*, *12*(2), 489–512. https://doi.org/10.5194/bg-12-489-2015

Breitburg, D., Levin, L. A., Oschlies, A., Grégoire, M., Chavez, F. P., Conley, D. J., et al. (2018). Declining oxygen in the global ocean and coastal waters. *Science*, *359*(6371). https://doi.org/10.1126/science.aam7240

Bronselaer, B., Russell, J. L., Winton, M., Williams, N. L., Key, R. M., Dunne, J. P., et al. (2020). Importance of wind and meltwater for observed chemical and physical changes in the Southern Ocean. *Nature Geoscience*, *13*(1), 35–42. https://doi.org/10.1038/s41561-019-0502-8

Buchanan, P. J., & Tagliabue, A. (2021). The regional importance of oxygen demand and supply for historical ocean oxygen trends. *Geophysical Research Letters*, *48*(20). https://doi.org/10.1029/2021GL094797

Buckley, M. W., & Marshall, J. (2015). Observations, inferences, and mechanisms of Atlantic meridional overturning circulation variability: A review. *Reviews of Geophysics*, *54*(1), 5–63. https://doi.org/10.1002/2015RG000493.Received

Buizza, R., Brönnimann, S., Haimberger, L., Laloyaux, P., Martin, M. J., Fuentes, M., et al. (2018). The EU-FP7 ERA-CLIM2 project contribution to advancing science and production of earth system climate reanalyses. *Bulletin of the American Meteorological Society*, *99*(5), 1003–1014. https://doi.org/10.1175/BAMS-D-17-0199.1

Davila, X., Olsen, A., Lauvset, S. K., McDonagh, E. L., Brakstad, A., & Gebbie, G. (2023). On the origins of open ocean oxygen minimum zones. *Journal of Geophysical Research: Oceans*, *128*(8), 1–16. https://doi.org/10.1029/2023JC019677

Deacon, G. E. R. (1937). The hydrology of the southern ocean. *Discovery Reports*, *15*, 1–124. Retrieved from https://ci.nii.ac.jp/naid/10004495930/en/

Döös, K., Nilsson, J., Nycander, J., Brodeau, L., & Ballarotta, M. (2012). The world ocean thermohaline circulation. *Journal of Physical Oceanography*, *42*(9), 1445–1460. https://doi.org/10.1175/JPO-D-11-0163.1

Döös, K., & Webb, D. J. (1994). *The deacon cell and the other meridional cells of the southern ocean* (Vol. 24). https://doi.org/10.1175/1520-0485(1994)024⟨0429:TDCATO⟩2.0.CO;2

Fasham, M. J., Ducklow, H. W., & McKelvie, S. M. (1990). A nitrogen-based model of plankton dynamics in the oceanic mixed layer. *Journal of Marine Research*, *48*(3), 591–639. https://doi.org/10.1357/002224090784984678

Feely, R. A., Sabine, C. L., Schlitzer, R., Bullister, J. L., Mecking, S., & Greeley, D. (2004). Oxygen utilization and organic carbon remineralization in the upper water column of the Pacific ocean. *Journal of Oceanography*, *60*(1), 45–52. https://doi.org/10.1023/B

Ferrari, R., & Ferreira, D. (2011). What processes drive the ocean heat transport? *Ocean Modelling*, *38*(3–4), 171–186. https://doi.org/10.1016/j.ocemod.2011.02.013

Feucher, C., Portela, E., Kolodziejczyk, N., & Thierry, V. (2022). Subpolar gyre decadal variability explains the recent oxygenation in the Irminger Sea. *Communications Earth Environment*, *3*, 1–9. https://doi.org/10.1038/s43247-022-00570-y

Follows, M. J., Dutkiewicz, S., Grant, S., & Chisholm, S. W. (2007). Emergent biogeography of microbial communities in a model ocean. *Science*, *315*(5820), 1843–1846. https://doi.org/10.1126/science.1138544

Frölicher, T. L., Aschwanden, M. T., Gruber, N., Jaccard, S. L., Dunne, J. P., & Paynter, D. (2020). Contrasting upper and deep ocean oxygen response to protracted global warming. *Global Biogeochemical Cycles*, *34*(8). https://doi.org/10.1029/2020GB006601

Garcia, H. E., Weathers, K. W., Paver, C. R., Smolyar, I., Boyer, T. P., Locarnini, R. A., et al. (2019). World ocean atlas 2018 volume 3: Dissolved oxygen, apparent oxygen utilization, and dissolved oxygen saturation. *NOAA Atlas NESDIS 83*, Vol. *3*, 38pp.

Gnanadesikan, A., Russell, J. L., & Zeng, F. (2007). How does ocean ventilation change under global warming? *Ocean Science*, *3*(1), 43–53. https://doi.org/10.5194/os-3-43-2007

Groeskamp, S., Lenton, A., Matear, R., Sloyan, B. M., & Langlais, C. (2016). Anthropogenic carbon in the ocean—Surface to interior connections. *Global Biogeochemical Cycles*, *30*(11), 1682–1698. https://doi.org/10.1002/2016GB005476

Hanawa, K., & Talley, L. D. (2001). Mode waters. In *International Geophysics Series*. 736pp (Vol. *77*, pp. 373–386). Retrieved from ftp://bslictb.nerc-bas.ac.uk/jbsall/Papers_CMIP5team/2001Hanawa.pdf

Hasumi, H., & Suginohara, N. (1995). Haline circulation induced by formation and melting of sea ice. *Journal of Geophysical Research*, *100*, (20), 613-620, 625. https://doi.org/10.1029/95JC02349

Helm, K. P., Bindoff, N. L., & Church, J. A. (2011). Observed decreases in oxygen content of the global ocean. *Geophysical Research Letters*, *38*(23), 1–6. https://doi.org/10.1029/2011GL049513

Herraiz-Borreguero, L., & Rintoul, S. R. (2011). Subantarctic mode water: Distribution and circulation. *Ocean Dynamics*, *61*(1), 103–126. https://doi.org/10.1007/s10236-010-0352-9

Heuzé, C. (2017). North Atlantic deep water formation and AMOC in CMIP5 models. *Ocean Science*, *13*(4), 609–622. https://doi.org/10.5194/os-13-609-2017

Holmes, R. M., Lavergne, C. D., & McDougall, T. J. (2019). Tracer transport within abyssal mixing layers. *Journal of Physical Oceanography*, *49*(10), 2669–2695. https://doi.org/10.1175/JPO-D-19-0006.1

Holmes, R. M., Zika, J. D., & England, M. H. (2019). Diathermal heat transport in a global ocean model. *Journal of Physical Oceanography*, *49*(1), 141–161. https://doi.org/10.1175/JPO-D-18-0098.1

Holzer, M. (2022). The fate of oxygen in the ocean and its sensitivity to local changes in biological production. *Journal of Geophysical Research: Oceans*, *127*(8). https://doi.org/10.1029/2022JC018802

IPCC. (2022). Changing ocean, marine ecosystems, and dependent communities. https://doi.org/10.1017/9781009157964.013

Ito, T., Follows, M. J., & Boyle, E. A. (2004). Is AOU a good measure of respiration in the oceans? *Geophysical Research Letters*, *31*(17), 1–4. https://doi.org/10.1029/2004GL020900

Jacobs, S. S. (2004). Bottom water production and its links with the thermohaline circulation. *Antarctic Science*, *16*(4), 427–437. https://doi.org/10.1017/S095410200400224X

Karstensen, J., Stramma, L., & Visbeck, M. (2008). Oxygen minimum zones in the eastern tropical Atlantic and Pacific oceans. *Progress in Oceanography*, *77*(4), 331–350. https://doi.org/10.1016/j.pocean.2007.05.009

Keeling, R. F., Körtzinger, A., & Gruber, N. (2010). Ocean deoxygenation in a warming world. *Annual Review of Marine Science*, *2*(1), 199–229. https://doi.org/10.1146/annurev.marine.010908.163855

Khatiwala, S., Primeau, F., & Holzer, M. (2012). Ventilation of the deep ocean constrained with tracer observations and implications for radiocarbon estimates of ideal mean age. *Earth and Planetary Science Letters*, *325–326*, 116–125. https://doi.org/10.1016/j.epsl.2012.01.038

Kolodziejczyk, N., Reverdin, G., & Lazar, A. (2015). Interannual variability of the mixed layer winter convection and spice injection in the eastern subtropical North Atlantic. *Journal of Physical Oceanography*, *45*(2), 504–525. https://doi.org/10.1175/JPO-D-14-0042.1

Laloyaux, P., de Boisseson, E., Balmaseda, M., Bidlot, J. R., Broennimann, S., Buizza, R., et al. (2018). CERA-20C: A coupled reanalysis of the twentieth century. *Journal of Advances in Modeling Earth Systems*, *10*(5), 1172–1195. https://doi.org/10.1029/2018MS001273

Lumpkin, R., & Speer, K. (2007). Global ocean meridional overturning. *Journal of Physical Oceanography*, *37*(10), 2550–2562. https://doi.org/10.1175/JPO3130.1

Luyten, J., Pedlosky, J., & Stommel, H. (1983). *Climatic inferences from the ventilated thermocline* (Vol. 5). https://doi.org/10.1007/BF02423489

Marshall, J., & Speer, K. (2012). Closure of the meridional overturning circulation through southern ocean upwelling. *Nature Geoscience*, *5*(3), 171–180. https://doi.org/10.1038/ngeo1391

McCartney, M. S., & Talley, L. D. (1982). *The subpolar mode water of the North Atlantic ocean* (Vol. 12). https://doi.org/10.1175/1520-0485(1982)012⟨1169:tsmwot⟩2.0.co;2

Morrison, A. K., Waugh, D. W., Hogg, A. M. C., Jones, D. C., & Abernathey, R. P. (2022). Ventilation of the southern ocean pycnocline. *Annual Review of Marine Science*, *14*(1), 405–430. https://doi.org/10.1146/annurev-marine-010419-011012

Oschlies, A., Brandt, P., Stramma, L., & Schmidtko, S. (2018). Drivers and mechanisms of ocean deoxygenation. *Nature Geoscience*, *11*(7), 467–473. https://doi.org/10.1038/s41561-018-0152-2

Portela, E., Kolodziejczyk, N., Maes, C., & Thierry, V. (2020). Interior water-mass variability in the southern hemisphere oceans during the last decade. *Journal of Physical Oceanography*, *50*(2), 361–381. https://doi.org/10.1175/JPO-D-19-0128.1

Portela, E., Kolodziejczyk, N., Vic, C., & Thierry, V. (2020). Physical mechanisms driving oxygen subduction in the global ocean. *Geophysical Research Letters*, *47*(17), 1–10. https://doi.org/10.1029/2020GL089040

Resplandy, L., Lévy, M., Bopp, L., Echevin, V., Pous, S., Sarma, V. V. S. S., & Kumar, D. (2012). Controlling factors of the oxygen balance in the Arabian Sea's OMZ. *Biogeosciences*, *9*(12), 5095–5109. https://doi.org/10.5194/bg-9-5095-2012

Rintoul, S. R. (2000). Southern ocean currents and climate. *Papers and Proceedings of the Royal Society of Tasmania*, *133*, 41–50. https://doi.org/10.26749/rstpp.133.3.41

Rousset, C., Vancoppenolle, M., Madec, G., Fichefet, T., Flavoni, S., Barthélemy, A., et al. (2015). The Louvain-la-Neuve sea ice model LIM3.6: Global and regional capabilities. *Geoscientific Model Development*, *8*(10), 2991–3005. https://doi.org/10.5194/gmd-8-2991-2015

Sarmiento, J. L., Hughes, T. M., Ronal, J. S., & Manabe, S. (1998). Simulated response of the ocean carbon cycle to anthropogenic climate warming. *Nature*, *393*(6682), 245–249. https://doi.org/10.1038/30455

Schmidtko, S., Stramma, L., & Visbeck, M. (2017). Decline in global oceanic oxygen content during the past five decades. *Nature*, *542*(7641), 335–339. https://doi.org/10.1038/nature21399

Speer, K., Rintoul, S. R., & Sloyan, B. (2000). The diabatic deacon cell. *Journal of Physical Oceanography*, *30*(12), 3212–3222. https://doi.org/10.1175/1520-0485(2000)030⟨3212:TDDC⟩2.0.CO;2

Sulpis, O., Trossman, D., Holzer, M., Jeansson, E., Lauvset, S. K., & Middelburg, J. J. (2023). Respiration patterns in the dark ocean. *Global and Planetary Change*, *37*(8), 1–21. https://doi.org/10.1029/2023GB007747

Talley, L. D., Reid, J. L., & Robbins, P. E. (2003). Data-based meridional overturning streamfunctions for the global ocean. *Journal of Climate*, *16*(19), 3213–3226. https://doi.org/10.1175/1520-0442(2003)016<3213:dmosft>2.0.co;2

Tamsitt, V., Drake, H. F., Morrison, A. K., Talley, L. D., Dufour, C. O., Gray, A. R., et al. (2017). Spiraling pathways of global deep waters to the surface of the southern ocean. *Nature Communications*, *8*, 1–10. https://doi.org/10.1038/s41467-017-00197-0

Zika, J. D., England, M. H., & Sijp, W. P. (2012). The ocean circulation in thermohaline coordinates. *Journal of Physical Oceanography*, *42*(5), 708–724. https://doi.org/10.1175/JPO-D-11-0139.1

Zika, J. D., Sijp, W. P., & England, M. H. (2013). Vertical heat transport by ocean circulation and the role of mechanical and haline forcing. *Journal of Physical Oceanography*, *43*(10), 2095–2112. https://doi.org/10.1175/JPO-D-12-0179.1

Zika, J. D., Sommer, J. L., Dufour, C. O., Molines, J. M., Barnier, B., Brasseur, P., et al. (2013). Vertical eddy fluxes in the southern ocean. *Journal of Physical Oceanography*, *43*(5), 941–955. https://doi.org/10.1175/JPO-D-12-0178.1

Erratum

The originally published version of this article contained two typographical errors in the Plain Language Summary. In the second sentence, beginning "In this study . . ." the phrase "using a sing a physical-biogeochemical model" should read "using a physical-biogeochemical model." The eighth sentence, beginning "The latter, loses about 25% of its oxygen during its journey" should read "The latter loses about 25% of its oxygen during its journey." The errors have been corrected, and this may be considered the authoritative version of record.